Received: 15 May 2018 | Accepted: 4 July 2018
DOI: 10.1002/maco.201810302

ARTICLE

Materials and Corrosion

Effect of the pH of the electrolyte on the formation and on the corrosion properties of ceria based coating on carbon steel

Nadjette Bourenane[1] | Youcef Hamlaoui[1] | Celine Remazeilles[2] | Fernando Pedraza[2]

[1] Laboratoire de Physique de la Matière et Rayonnement (LPMR), Faculté des Sciences et de Technologie, Université Mohamed Chérif Messaadia, BP 1553, 41000 Souk-Ahras, Algeria

[2] Laboratoire de Sciences de l'Ingénieur pour l'Environnement (LaSIE), UMR 7356 CNRS Pôle Science et Technologie, Université de la Rochelle, Avenue Michel Crepeau, 17042 La Rochelle Cedex 1, France

Correspondence
Youcef Hamlaoui, Laboratoire de Physique de la Matière et Rayonnement (LPMR), Faculté des Sciences et de Technologie. Université Mohamed Chérif Messaadia. BP 1553. 41000 Souk-Ahras. Algeria.
Email: hamlaoui_youcef@yahoo.fr

The effects of the modification of the pH in 0.1 M cerium nitrate solutions in the elaboration and corrosion resistance of ceria based coatings on carbon steel are investigated. Increasing the concentration of acetic acid impedes an efficient electrodeposition. At low concentrations, acetic acid seems to prevent the precipitation of $Ce(OH)_3$ and the formation of even films of cerium oxides is favored. The increase of pH through the addition of NaOH to the cerium nitrate solutions with 0.008 M of acetic acid is shown to provide superior corrosion resistance for exposures in air and immersed in 0.5 M NaCl for 30 days.

KEYWORDS
cathodic electrodeposition, cerium oxide coatings, corrosion, corrosion products, morphology solution pH

1 | INTRODUCTION

Rare earth metals are among the best alternatives to the toxic hexavalent chromium either as conversion coatings or corrosion inhibitors. Hinton et al.[1] were the first authors to carry out the deposition of rare earth metals. Various coating techniques can be adopted regarding the application of these rare earth metals based coatings on different metal substrates (Al, stainless steels, zinc, etc.) to be protected. For instance, physical, chemical, or electrochemical techniques like simple immersion, anodic or cathodic deposition, PVD, sol-gel, etc., have been reported to successfully elaborate such coatings.[2–12]

The final coating is composed of two layers (inner and outer) with different chemistries. While it is established that the outer layer is mainly composed of cerium oxy-hydroxides,[13] the chemistry of the inner layer depends on the metal substrate and on the application technique.[12–14] Indeed, in addition to the cerium (III) hydroxide, the inner layer of the coating is usually enriched with different amounts of the chemical dissolution products of the substrate due to the acidic pH of the deposition solution. For some materials, the presence of this type of corrosion products does not affect the quality of the coating. For instance, it is well known that the dissolution products of, for example, Al, and Cr are homogeneous, compact, and adhere well to the surface of the substrate and consequently constitute a corrosion barrier to prevent aggressive media to penetrate through. In contrast, the corrosion products formed on zinc impair little protection.[15,16]

In the case of mild steel, the $Ce(NO_3)_3$ concentrations employed to deposit cerium oxyhydroxides have pH values between 3.1 and 4.5.[17] Such acidic pHs promote the formation of ferrous hydroxide $Fe(OH)_2$ and carbonated green rusts that oxidize further in lepidocrocite.[18] Most of such iron-based corrosion products are known to be not protective due to their porosity and low adhesion to the steel substrate.[19] Yet, cerium oxides films have been reported to act as effective cathodic coating and to restore the passive state of steel after being disturbed in NaCl 3.5% solution "self-healing mechanism"

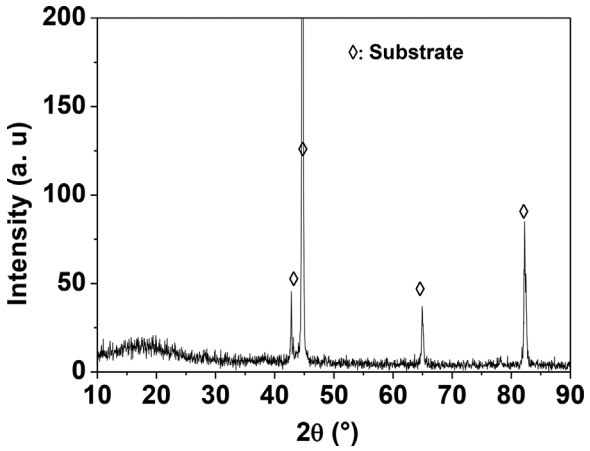

FIGURE 1 XRD pattern of steel substrate after electrodeposition from 0.1 M $Ce(NO_3)_3$ with (0.1 M) acetic acid addition at room temperature and 0.5 mA/cm^2 as applied current density for 20 min

through the formation of secondary layer of $Ce(OH)_4$, CeO_2, $Fe(OH)_2$, and Fe_2O_3 in scratched area.[20]

Therefore, the use of additives in the electrodeposition bath is often recommended. Generally, small amounts of additives affect mainly the electrodeposition reaction kinetics either by adsorption or complexation.[21–22] Thus, an important part of metal and metal oxide electrodeposition is realized from baths containing organic additives.[23–27] In the particular case of an efficient cathodic electrodeposition of the cerium oxides, it is necessary to stabilize Ce^{3+} ion to prevent the precipitation of $Ce(OH)_3$ according to reactions (1) to (3)[28,29]:

$$2\ Ce^{3+} + 3\ H_2O \rightleftarrows Ce(OH)_3 + 6\ H^+ \quad (1)$$

$$2\ Ce^{3+} + 3\ H_2O \rightleftarrows Ce_2O_3 + 6\ H^+ \quad (2)$$

$$Ce_2O_3 + H_2O \rightleftarrows 2\ CeO_2 + 2\ H^+ + 2e^- \quad (3)$$

In some of our previous works[30,31] we have shown that the coatings obtained from a bath containing cerium nitrate and an organic additive (polyethylene glycol, PEG) on electrogalvanized steel and in mild steel were somewhat free from corrosion products and showed a good resistance against corrosion for long immersion times in NaCl and Na_2SO_4 solutions. Ferreira et al.[32] obtained a uniform protective coating composed of CeO_2 dominated by Ce_2O_3 on electrogalvanized steel through the addition of citric acid. Golden and Wang employed lactic, acetic, citric, and oxalic acids and EDTA in the anodic deposition method of CeO_2.[33] They concluded that ligands with weaker formation constants, that is, acetic and lactic acid were able to produce CeO_2 films under certain experimental conditions. Indeed, ligands (chelants) such as EDTA and citric acid can strongly complex the metal[34] in which case, cerium would not be available to precipitate as cerium hydroxide. Therefore, in the present study, acetic acid is chosen since it forms metalorganic complex with Ce^{3+} and dissolve well in aqueous medium.[33] The aim is to obtain electrodeposits on carbon steel substrate free from corrosion products with good corrosion protectiveness. Thus, cathodic electrodeposition of cerium oxide was carried out on carbon steel from a bath containing 0.1 M cerium nitrate and acetic acid. The effect of the pH of the solution was also studied by adding NaOH drops. The corrosion protection performance of the final electrodeposited films was evaluated in ambient air and in 0.5 M NaCl solution for 30 days.

2 | EXPERIMENTAL PROCEDURE

2.1 | Materials

Round samples of 14 mm of diameter and thickness of 2 mm of A 366 cold-rolled carbon steel (Fe-0.13C-0.041Mn-0.04 S-0.012N-0.55Cu, wt%-nominal composition) were polished with progressively finer grit of SiC till grade #4000, rinsed with distilled water and cleaned in ultrasonic bath of ethanol and dried with hot air immediately before electrodeposition.

2.2 | Experimental set-up for cathodic electrodeposition and electrochemical tests

A 0.1 M aqueous solution of $Ce(NO_3)_3 \cdot 6H_2O$ (Aldrich, ≥99% pure) was employed as electrodeposition bath (pH 3.87). Different concentrations (0.008–0.1 M) of acetic acid were added as complexing agent. The pH of the solutions was modified by adding drops of NaOH 1 M every 5 min. The electrodeposition was performed using a classical three-electrode configuration set-up, with the carbon steel sample being the cathode, a platinum grid as the counter electrode and a saturated calomel electrode (SCE) as the

TABLE 1 pH of the different solutions and of the calculated concentrations of cerium acetate and of protons

[HA] (M)	0.008	0.01	0.03	0.06	0.1
pH with 0.1 M Ce + HA	3.17	3.15	3.00	2.87	2.73
$[Ce(CH_3COO)_3]$(M)	2.4 10^{-4}	3.3 10^{-3}	8.9 10^{-3}	1.7 10^{-2}	1.9 10^{-2}
$[H^+]$(M)	7.1 10^{-4}	9.9 10^{-3}	2.7 10^{-2}	5.2 10^{-2}	5.6 10^{-2}

NB: HA = acetic acid.

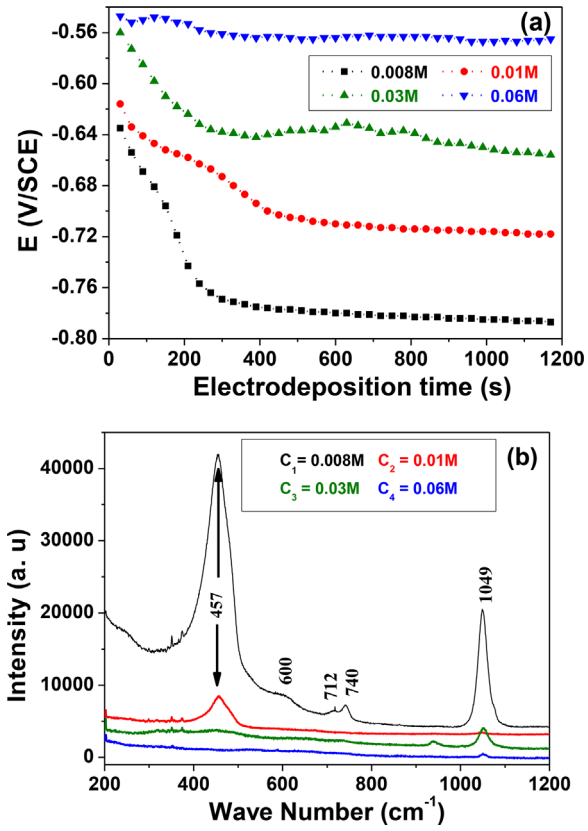

FIGURE 2 (a) Evolution of the potential with time and (b) Raman spectra for deposits performed at 0.5 mA/cm^2, for 20 min in 0.1 M $Ce(NO_3)_3$ with increasing acetic acid concentrations (C1) 0.008, (C2) 0.01, (C3) 0.03, and (C4) 0.06 M. [Color figure can be viewed at wileyonlinelibrary.com]

reference one. The measurements were carried out using a potentiostat/galvanostat AutoLab PGZ 300. The same experimental set-up was used for the corrosion tests in 0.5 M NaCl (Fluka, ≥99.5% pure). Cyclic voltammetry was recorded from −1.0 to −2.5 V/SCE at 10 mV/min as scanning rate. All the corrosion tests were repeated two or three times for reproducibility purposes. They were carried out at room temperature by magnetic stirring the solutions to obtain a slight vortex of the electrolyte. Prior to any electrochemical test, the time to stabilization of the open circuit potential was 30 min. The Tafel polarization curves were obtained at a scanning rate of 10 mV/min around ±250 mV with respect the open circuit potential (*Eocp*). Polarization resistance (*Rp*) was carried out at 10 mV/min of scan rate, and the derived values were obtained at 20 mV away (cathodic and anodic domains) of the corrosion potential (*Ecorr*).

2.3 | Characterization of the films

The morphologies of the films were first investigated by optical microscopy (LEICA DM R-MN) then by scanning electron microscopy (SEM) (JEOL 5410 LV). The

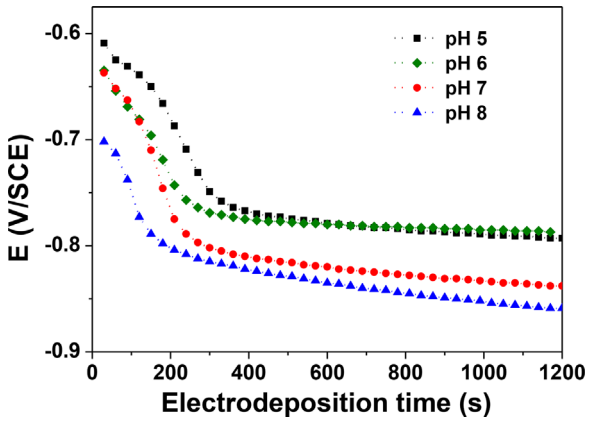

FIGURE 3 Evolution of the potential with time for deposits performed at 0.5 mA/cm^2 for 20 min in 0.1 M $Ce(NO_3)_3$ + 0.008 M acetic acid with pH adjusted by NaOH additions. [Color figure can be viewed at wileyonlinelibrary.com]

structural features of the deposits were investigated by X-ray diffraction (XRD) in the θ–2θ configuration using Cu Kα radiation $\lambda = 1.5406$ nm (Bruker AXS D8-Advanced diffractometer). The different components were analyzed by Raman microspectroscopy (Jobin Yvon LabRam HR8000) using an incident beam of 632.82 nm emitted by a HeNe laser. Different spots ~3 μm on the surface were analyzed after focusing with the ×50 lens of the optical microscope (Olympus BX 41) attached to the apparatus. The resolution of the spectra is about 2 cm^{-1} at room temperature. The characteristic bonds were identified by Fourier transformed infrared spectroscopy with a Thermo Nicolet FT-IR Nexus spectrometer using a KBr beamsplitter, a DTGS detector and a diffuse reflectance accessory. The powders of the deposit were mixed by grinding with a mirror. The spectra were recorded with the Omnic software at a resolution of 4 cm^{-1} and an accumulation of 64 scans. The background was carried out with KBr. The deposits were also scraped, then milled, and further analyzed by differential scanning calorimetry (DSC) in a Q100 of TA instruments between 30 and 550 °C with a heating rate of 10 °C min^{-1} under nitrogen.

2.4 | Experimental set-up for electrochemical tests

For the electrochemical tests, the same experimental set-up used in the electrodeposition tests was employed.

3 | RESULTS AND DISCUSSION

3.1 | Characterization of the deposits

The influence of the addition of different concentrations of acetic acid on the deposition of cerium hydroxide was

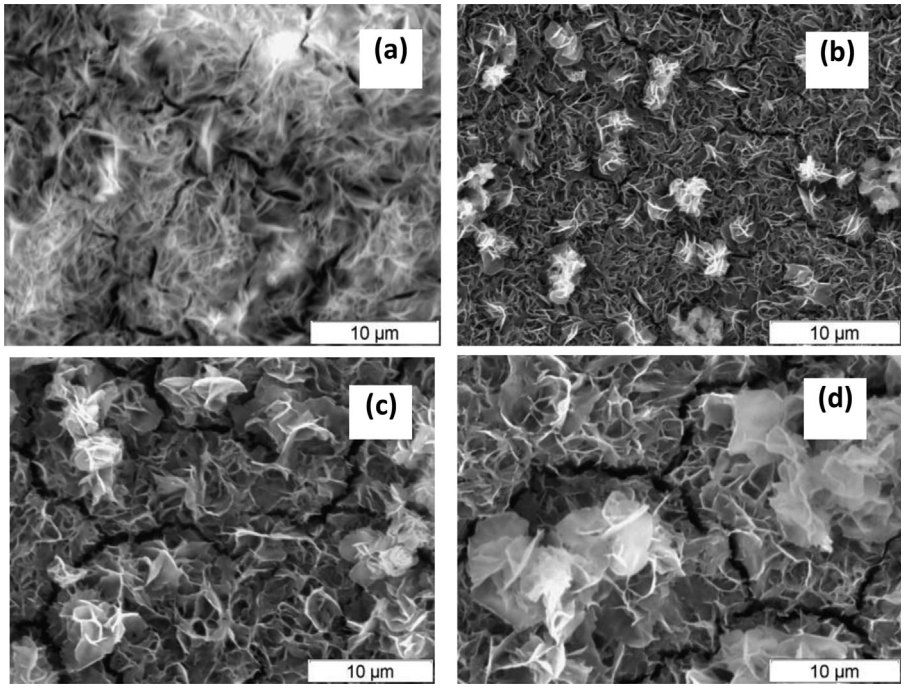

FIGURE 4 SEM images of the deposits obtained at −0.5 mA/cm^2 for 20 min from 0.1 M $Ce(NO_3)_3$ and 0.008 M acetic acid with increasing pH (a) 5; (b) 6; (c) 7; and (d) 8 at room temperature.

investigated. With the addition of 0.1 M of acetic acid, the pH of the cerium nitrate solution dropped from 3.87 to 2.73. After several tests of electrodeposition at −0.5 mA/cm^2 for 20 min (1200 s), the pH remained unchanged (2.73), which suggested that no film had formed. This was confirmed by XRD, where no peaks related to CeO_2 or $Ce(OH)_3$ were detected (Figure 1). Therefore, the concentration of acetic acid was decreased to (C1) 0.008 (pH 3.17), (C2) 0.01 (pH 3.15), (C3) 0.03 (pH 3.00), and (C4) 0.06 M (pH 2.87) (Table 1).

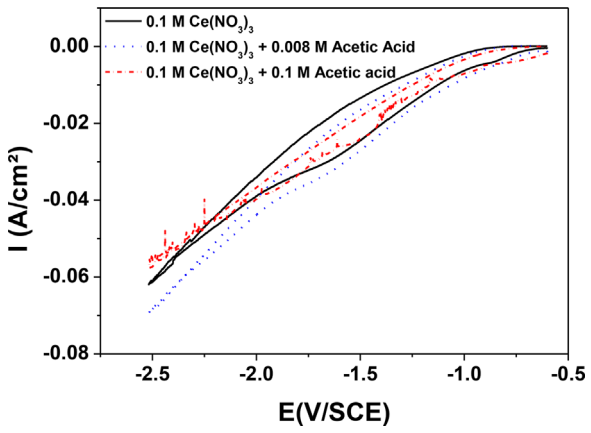

FIGURE 5 Cyclic voltammograms (scanning rate 20 mV/s) for carbon steel in 0.1 M cerium nitrate solution with and without addition of acetic acid. [Color figure can be viewed at wileyonlinelibrary.com]

According to the literature,[32,33] the reaction between the cerium salt and acetic acid occurs through Eq. (4):

$$Ce^{+3} + xL^- \rightarrow CeL_x^{(3-x)+} \quad (4)$$

where L is here the acetate ion (CH_3COO^-)

This reaction is characterized by a single constant of formation with Log $\beta = 1.68$[33] following Eq. (5):

$$Ce^{+3} + 3\ CH_3COOH \rightleftarrows Ce(CHCOO)_3 + 3\ H^+ \quad (5)$$

Hence, for any concentration of acetic acid, for example, 0.008 M:

$$Ce^{3+} + 3\ CH_3COOH \rightarrow \left[Ce(CH_3COO)_3\right] + 3\ H^+$$

at $t = 0$	0.1 M	0.008 M	0	0
at equilibrium	0.1–x	0.008–3x	x	3x

Therefore,

$$K_f = \frac{\left[Ce(CH_3COO)_3\right][H^+]^3}{[Ce^{3+}][CH_3COOH]^3} \Rightarrow \left[Ce(CH_3COO)_3\right] = \mathrm{Kf}\frac{(0.1-x)\left(\left[Ce(CH_3COO)_3\right]-3x\right)^3}{(3x)^3} \quad (6)$$

with $\log K_f = 1.68$ [33] $\Rightarrow K_f = 10^{1.68} = 47.86$

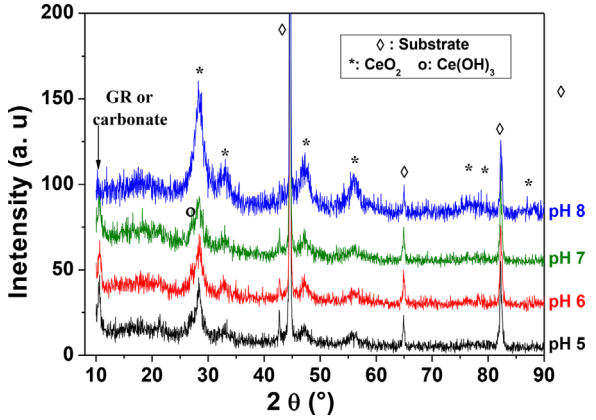

FIGURE 6 XRD pattern of the cerium oxide film elaborated in 0.1 M $Ce(NO_3)_3$ + 0.008 M acetic acid at room temperature and -0.5 mA/cm^2 for 20 min at different solution pH. [Color figure can be viewed at wileyonlinelibrary.com]

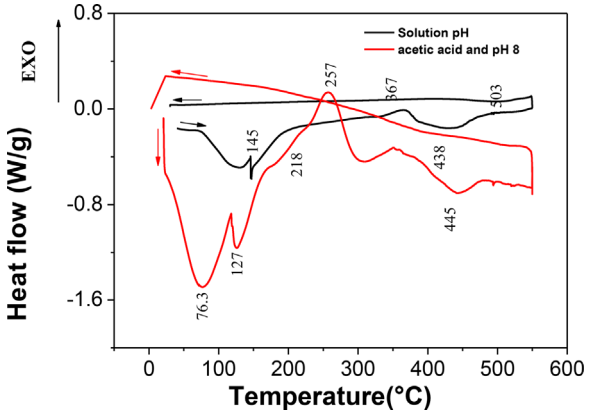

FIGURE 8 DSC curves of the powders scraped from the deposits elaborated at -0.5 mA/cm^2 for 20 min from 0.1 M $Ce(NO_3)_3$ and from 0.1 M $Ce(NO_3)_3$ + 0.008 M acetic acid at pH 8. [Color figure can be viewed at wileyonlinelibrary.com]

This results in $[Ce(CH_3COO)_3] = 2.4\ \ 10^{-4}$ M and $[H^+] = 7.1\ 10^{-4}$ M. Similarly, the concentrations of cerium acetate and of protons can be calculated for the different concentrations of acetic acid added to the cerium nitrate solution (Table 1).

Since cathodic electrodeposition occurs through the local alkalinization of the interface,[9] the lowest concentration of acetic acid (0.008 M) allowed to maintain a relatively high pH (3.13) that facilitated the homogeneous deposition. In contrast, the increase of the acetic acid concentration is detrimental to the cerium coating as observed through the absence of decrease of potential toward more negative (cathodic) values (Figure 2a). This behavior was confirmed by Raman spectroscopy (Figure 2b). Irrespective of the concentration of acetic acid, all the Raman spectra showed the symmetric vibration of Ce—O bond at 457 cm^{-1} whose intensity decreased with increasing acid concentration. In addition, the shift of this bond from 457 to 450 cm^{-1} with low acid concentration could be related to the evolution of the particle size of CeO_2 and/or to oxygen vacancies in the deposits.[35] This hypothesis is supported by the band at 600 cm^{-1} typical of oxygen vacancies.[29] The peak at 712 cm^{-1} is related in the literature to carbonates[17] while the peaks at 740–1049 cm^{-1} can be ascribed to nitrates.[18]

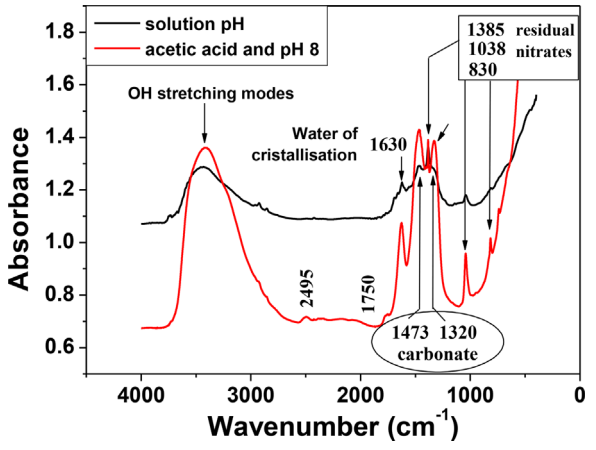

FIGURE 7 FT-IR spectra of the powders scraped from the deposits elaborated at -0.5 mA/cm^2 for 20 min from 0.1 M $Ce(NO_3)_3$ and from 0.1 M $Ce(NO_3)_3$ + 0.008 M acetic acid at pH 8. [Color figure can be viewed at wileyonlinelibrary.com]

Therefore, the bath containing 0.1 M of $Ce(NO_3)_3 \cdot 6H_2O$ and low concentration of acetic acid ($C_1 = 0.008$ M, pH 3.17) was selected to study the effect of the increase of the pH solution on its chemical stability in time until 7 days by adding NaOH drops every 5 min. Between pH 5 and 8 the color of the solution did not evolve from transparent to green or yellow, which are respectively, typical of $Ce(OH)_3$ and CeO_2,[33] that is, there was no precipitation of the cerium compounds in the solution.

The evolution of the potential with electrodeposition time and with increasing pH from 5 to 8 and applied current density of 0.5 mA/cm^2 is shown in Figure 3. All curves display a sudden decrease of the potential in the first period ($t < 250$ s) followed by a stabilization period which is attributed to the formation of a film covering the whole surface of the substrate.[29] The shift of the potentials to more negative values is related to the increase of the film thickness.[36] These phenomena are more marked with increasing the pH of the solution. Moreover, the shape of the curves looks similar irrespective of the pH, which suggests that the growth mechanisms of the deposits are equivalent.[37]

The SEM images show a surface totally covered with a deposit of acicular and laminated structure (Figure 4). The needle-like morphology is typical of hydroxide bonding[29] while the laminated is associated with the oxide.[17] The latter increases with increasing the pH, that is, the more alkaline the solutions the more favored is the oxide. However, cracking of the coatings is also promoted with increasing pH. The cracks

TABLE 2 Thermal data for the indicated systems

	Solution pH			Acetic acid and pH 8		
Transformation	T_{max} (°C)	ΔT (°C)	ΔH (J/g)	T_{max} (°C)	ΔT (°C)	ΔH (J/g)
Water release amorphous phase	130 145	[110–141] [150–159]	5.62 6.61	76 127	[60–93] [120–139]	9.28 4.12
Acid acetic decomposition	–	–	–	257	[257–274]	29.75
Ce^{3+} to Ce^{4+}	367	[324–336]	0.097	367	[287–330]	2.13
$Ce(OH)_4$ to CeO_2	438	[418–451]	2.17	445	[427–463]	3.99

can be generated by the shear stresses between the coating and the substrate[38] or by the hydrogen evolution reaction (HER) that induce stresses in the coating itself.[39]

The cyclic polarization curves obtained from cerium nitrate solution with and without acetic acid addition confirmed this hypothesis (Figure 5). The potential shifts toward more cathodic values and the hysteresis is more important with 0.008 M than with 0.1 M of acetic acid. Moreover, the addition of 0.008 M of acetic acid results in a hysteresis similar to the 0.1 M $Ce(NO_3)_3 \cdot 6H_2O$ solution. The shift of the potential and the hysteresis was already observed in acetic acid-free 0.1 M $Ce(NO_3)_3 \cdot 6H_2O$ solutions[29] and was ascribed to the formation of the cerium hydroxide then to the cerium oxide by oxidation of the Ce^{3+} compounds. However, the deposits contained cracks. Here, the low concentrations of acetic acid allowed to retain minute amounts of Ce (III) that can be released from the complex according to Eq. (8), that is, the reverse of Eq. (4).[33] The maximum concentration of $[Ce^{3+}]$ that can be released is given by that of the cerium acetate (Table 1).

$$2\ \mathrm{Ce(III)} - \mathrm{L} \rightleftarrows 2\ \mathrm{Ce}^{3+} + 2\ \mathrm{L} \tag{7}$$

In contrast, with the high concentration of acetic acid (0.1 M), the deposit cannot form because of the HER following reactions (8) and (9)[40]:

$$\mathrm{Fe} + \mathrm{HAc} + \mathrm{le}^- \rightleftarrows \mathrm{FeH} + \mathrm{Ac}^- \tag{8}$$

$$\mathrm{FeH} + \mathrm{Hads} \rightleftarrows \mathrm{H_2} + \mathrm{Fe} \tag{9}$$

where HAc and Ac^- are, respectively, the acetic acid and the acetate anion.

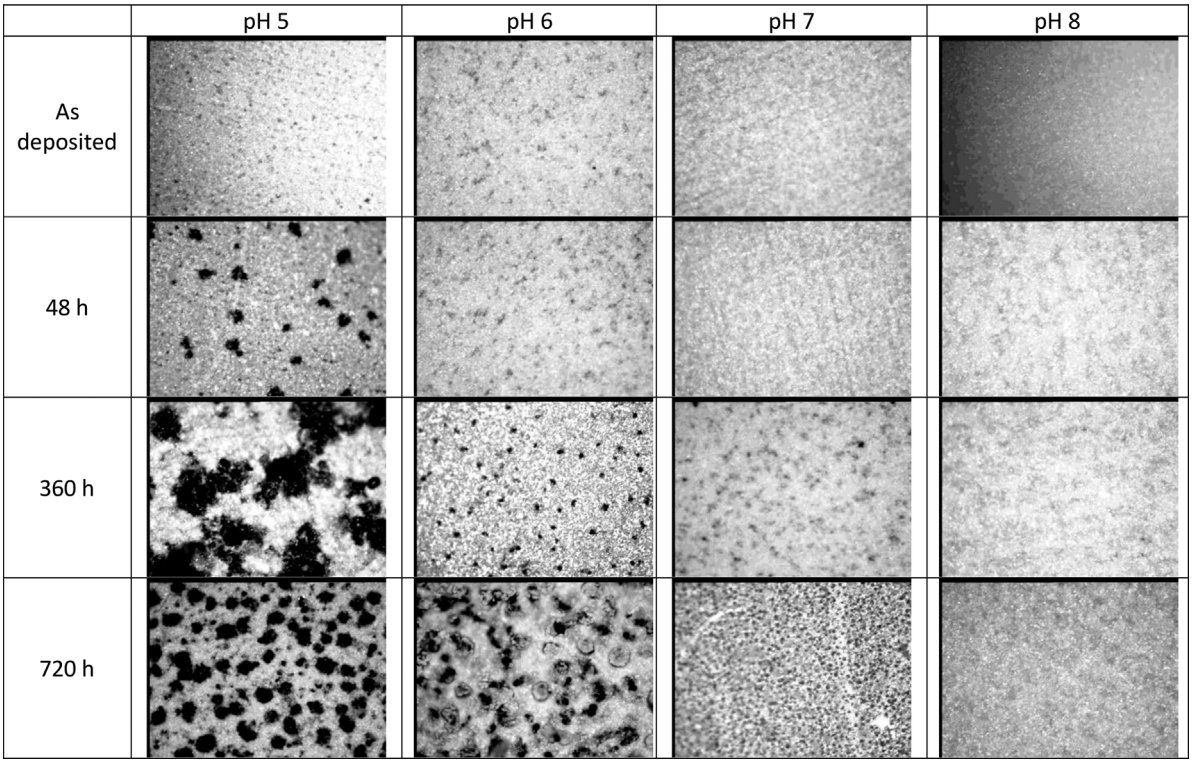

FIGURE 9 Optical micrographs (X30) showing the evolution of the surface of the deposits obtained from 0.1 M $Ce(NO_3)_3$ + 0.008 M acetic acid at different pH and exposures to ambient air.

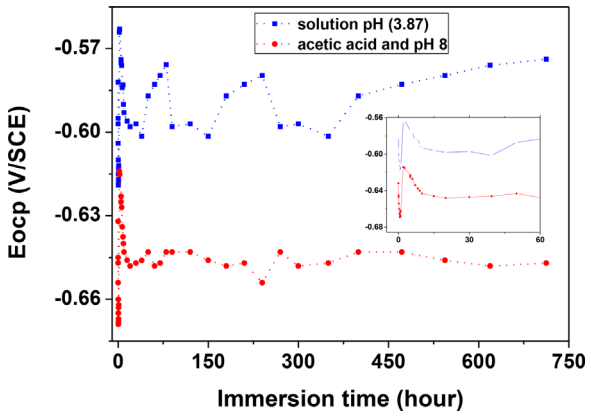

FIGURE 10 Evolution of the *Eocp* with immersion time for ceria based coating prepared from cerium nitrate at solution pH and from cerium nitrate with the addition of acetic acid and pH 8. [Color figure can be viewed at wileyonlinelibrary.com]

Indeed, the release of gas bubbles was observed at the naked eye and the E versus time curves appear noisy.

Irrespective of the pH and with 0.008 M of acetic acid, all the patterns display the typical fluorite structure of CeO_2 in addition to the peaks of the substrate (Figure 6). However, at pH 5–7, two additional peaks appear at 10.5 and 22° which can be related to the carbonated green rust.[41] In contrast, such green rust is not observed at pH 8. Viricelle reports that the peak at 10.4° corresponds to $Ce_2(CO_3)_3 \cdot 8H_2O$.[42] Therefore, FT-IR analyses were performed for a more thorough assessment of the compound formed at pH 8 (Figure 7). The peaks at 830, 1038, and 1385 cm^{-1} are associated with nitrates while those at 1320 and 1473 cm^{-1} correspond to carbonates when compared to the FT-IR spectra of $Ce(NO_3)_3 \cdot 6H_2O$ and $Ce_2(CO_3)_3 \cdot 8H_2O$.[42] Therefore, it appears that the XRD peak at 10.5° corresponds rather to carbonate species instead of the green rust. In addition, the peaks located at 1320, 1750, and 2495 cm^{-1} can be assigned to C—O, C═O stretching vibration, and C-H asymmetric stretching in CH_3 in plane bending, respectively.[43,44] The strong and wide bond appearing at 3300 cm^{-1} is assigned to OH^- stretching. All the latter are indicative of the presence of the molecular form of acetic acid whether adsorbed on the surface of the electrode or entrapped in the deposits.

The presence of acetic acid in the deposit was investigated by DSC (Figure 8). Table 2 gathers the main results of the thermal characterization such as humidity, amorphous phase, decomposition, transformation as well as the temperature ranges. In general, both curves display the same phenomena upon heating which consist first in the release of water and in the transformation from the amorphous hydroxide into crystalline ceria.[17] However, the exact temperature and the energy associated with the thermal events are different at pH 8 than at the solution pH. In particular, water seems to be released of the pH 8 deposits at 76 °C while dehydration occurs at about 130 °C in the deposits obtained at the solution pH. Similarly, the temperature at which the transformation from the amorphous to crystalline phase occurs is lower in the deposits obtained at pH 8. This is indicative of a more crystallized deposit at pH 8. Also, an additional intense exothermic peak at 257 °C is observed at pH 8 that can be attributed to the decomposition of acetic acid[45] although Viricelle attributes the thermal evolution at 270 °C to $CeOHCO_3$ issued from the hydrolysis of $Ce_2(CO_3)_3 \cdot 8H_2O$ with acetic acid.[43] In addition, the transformation of Ce(III) and Ce(IV) hydroxides to Ce(IV)

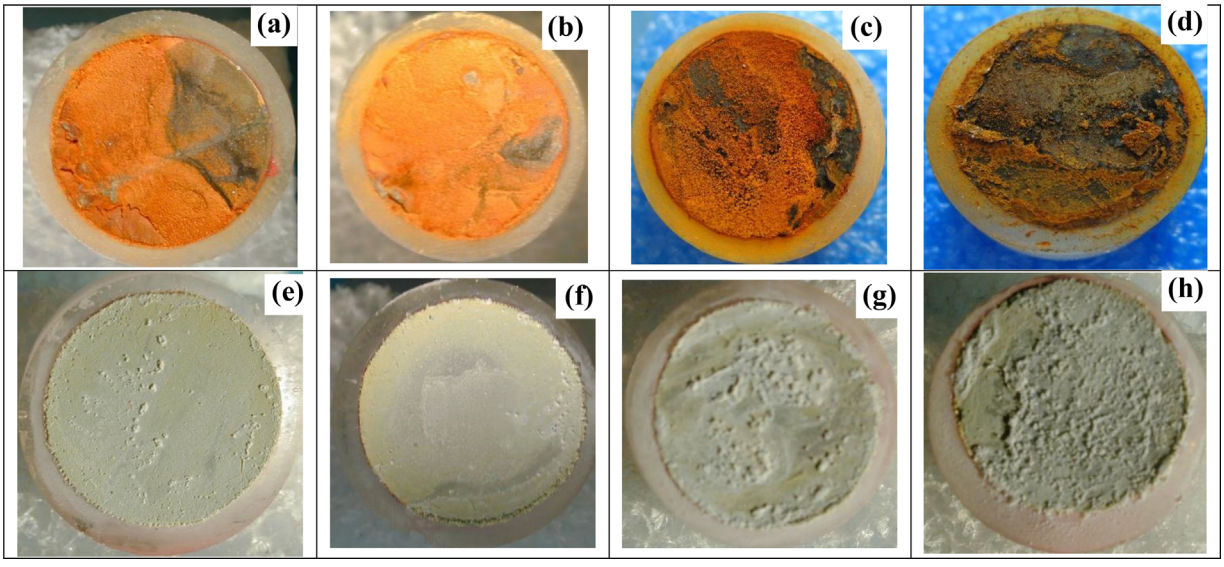

FIGURE 11 Evolution of the surface of the deposits with immersion time in 0.5 M NaCl. (a,e) 48 h; (b,f) 240 h; (c,g) 480 h; and (d,h) 720 h. (a–d) correspond to the deposits elaborated at the solution pH. (e–h) to the deposits elaborated with acetic acid and pH 8. (All elaborated at −0.5 mA/cm^2 for 20 min in 0.1 M $Ce(NO_3)_3$). [Color figure can be viewed at wileyonlinelibrary.com]

oxide at pH 8 is accompanied by a greater absorption of energy which indicates that the oxidation of the deposits prepared at pH 8 occurs more slowly compared to those obtained at the solution pH (3.87). In summary, it appears that the deposits formed with acetic acid and pH 8 contain less water, are more oxidized, that is, CeO_2 and probably contain carbonates, nitrates, and acetic acid.

3.2 | Protection afforded by the deposits

The protection afforded by these electrodeposits was conducted by exposing the coated samples to ambient air for 30 days (720 h) and room temperature. As opposed to the coatings obtained at different pHs, the one at pH 8 did not show any corrosion product at the surface (Figure 9). In agreement with our previous work,[46] we can conclude that the substrate dissolution occurs just after immersion of the electrode in the solution which leads to the formation of rust beneath the ceria based coating.

This positive result encouraged us to assess electrochemically the coating obtained from 0.1 M $Ce(NO_3)_3$ at pH 8. Potentiodynamic polarization tests were carried out in 0.5 M NaCl for 720 h (30 days). Figure 10 presents the typical chronopotentiometric curves obtained for the samples coated at pH 8 and at the solution pH (3.87). At the solution pH, the *Eocp* shifted strongly toward more cathodic values at the initial stage of immersion. Then, the *Eocp* moved to anodic direction reaching the steel substrate potential (−0.492 mV/SCE). The fluctuation of *Eocp* between 50 and 350 h close to the potential of steel can be related to a transient stage in which the establishment and dissolution of corrosion film on the substrate surface are concomitant.[47] Between 350 and 500 h, the *Eocp* evolved toward the substrate potential. These results indicate that the sample is still under active corrosion process where the coating is unable to provide protection.

However, the *Eocp* for the coatings prepared at pH 8, is lower than that for coating obtained at solution pH. As with the solution pH, the *Eocp* evolves during the first hour but the potential value does not exceed the potential of the initial coating (−0.61V/SCE) and then stabilizes at −0.64V/SCE along the whole exposure. Since this *Eocp* is sufficiently far from the potential of the steel substrate, one can presume that the evolution during the first hours arises from the penetration of the aggressive solution through cracks and defects in the coating that ensures the self-healing ability of the ceria based coatings proposed by Ferreira et al. and Ma et al. [48,49]

In order to compare the appearance of the surface of both coatings after the immersion period, the evolution of the surface was examined by using optical microscopy (Figure 11). It can be clearly seen that the coatings prepared at solution pH show full degradation from 2 days of immersion in NaCl solution where the red rust (substrate dissolution) covers the whole surface. However, the coatings prepared with acetic acid and pH 8 continue to be resistant against corrosion throughout the whole testing period.

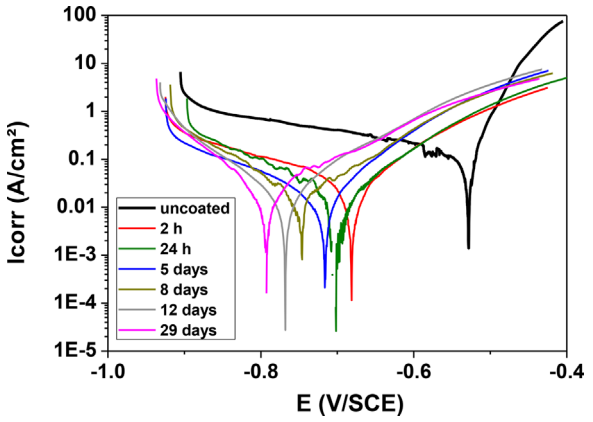

FIGURE 12 Polarization curves of the deposits obtained after 20 min of electrodeposition at 0.5 mA/cm^2 from 0.1 M $Ce(NO_3)_3$ + 0.008 M acetic acid and pH 8 as function of immersion time in 0.5 M NaCl. [Color figure can be viewed at wileyonlinelibrary.com]

Potentiodynamic polarization curves were performed during 30 days (720 h) of immersion in 0.5 M NaCl solution (Figure 12). The corresponding corrosion current densities "*Icorr*" using the Tafel extrapolation are depicted in Figure 13 and the data gathered in Table 3. Figure 12 shows that the *Ecorr* shifts continuously toward the cathodic domain with immersion time. In addition, the shape of the anodic branches of all the curves are less affected with time compared to the cathodic ones, which indicates that the corrosion process is under cathodic control. At the beginning of the immersion, the *Icorr* for the coated substrate was around 39 μA/cm^2 which is four times lower than the value of the untreated substrate (111 μA/cm^2). During the first 48 h, the *Icorr* dropped dramatically, then tended to increase slowly till a sharp increase at 360 h (15 days). Thereafter, the *Icorr* dropped

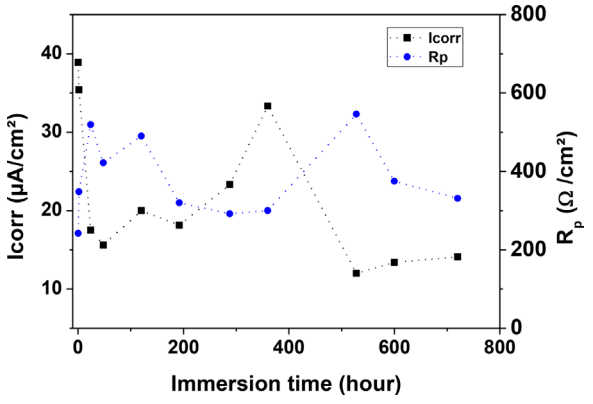

FIGURE 13 Evolution of *Icorr* and R_p as function of immersion time in 0.5 M NaCl for electrodeposits from 0.1 M $Ce(NO_3)_3$ + 0.08 M acetic acid and pH 8. [Color figure can be viewed at wileyonlinelibrary.com]

TABLE 3 Electrochemical parameters calculated from polarization measurements on uncoated and passivated mild steel electrode with ceria based coating in 0.1 M NaCl solution at room temperature

Exposure (hour)	E_{corr} (mV/SCE)	βc (mV/dec)	βa (mV/dec)	Rp (Ω . cm²)	I_{corr} (μA/cm²)
0	−530	261	111	120	148.9
2	−680	233	117	348	35.0
24	−704	132	105	519	17.5
48	−735	135	97	422	15.6
120	−717	92	103	743	20.1
192	−747	118	106	320	18.2
288	−769	93	120	292	23.2
360	−795	86	130	300	18.7
528	−803	87	113	546	12.0
600	−790	83	125	375	13.4
720	−793	84	131	331	14.1

again and remained stable till 720 h (30 days). Such fluctuations of the *Icorr* values suggest that the coating remains active till completely healed with corrosion products. This hypothesis is confirmed by the evolution of the polarization resistance *Rp* with time (Figure 13) that follows the opposite trend of *Icorr*.

4 | CONCLUSION

The addition of low concentrations of acetic acid to 0.1 M $Ce(NO_3)_3 \cdot 6H_2O$ solutions allow to prevent chemical precipitation of $Ce(OH)_3$ upon cathodic electrodeposition at $-0.5\ mA/cm^2$ for 20 min on a carbon steel substrate. The increase of pH by adding NaOH drops results in quite protective coatings in ambient air for 30 days. The cerium oxide based coatings seem to trap carbonates, nitrates and acetic acid. When immersed in 0.5 M NaCl, the coatings require at least 15 days (320 h) to stabilize. Then, the *Eocp*, *Icorr*, and *Rp* tend to being stable where they come to confirm the good electrochemical behavior of the coating obtained at pH 8 compared to those obtained at the solution pH.

ORCID

Youcef Hamlaoui http://orcid.org/0000-0003-0737-7401

REFERENCES

[1] B. R. W. Hinton, *Corros. Sci*. **1989**, *29*, 967.
[2] J. F. Jue, J. Jusko, A. V. Virkar, *J. Electrochem. Soc*. **1992**, *139*, 2458.
[3] M. J. Capitan, A. Paul, J. L. Pastol, J. A. Odriozola, *Oxid. Met*. **1999**, *52*, 447.
[4] P. L. Chen, I. W. Chen, *J. Am. Ceram. Soc*. **1993**, *76*, 1577.
[5] M. Hirano, E. Kato, *J. Am. Ceram. Soc*. **1996**, *79*, 777.
[6] N. Ozer, *Sol. Energy Mater. Sol. Cells*. **2001**, *68*, 391.
[7] C. Agrafiotis, A. Tsetsekou, C. J. Stournaras, A. Julbe, L. Dalmazio, C. Guizard, *J. Eur. Ceram. Soc*. **2002**, *22*, 15.
[8] P. Stefanov, G. Atanasova, D. Stoychev, T. S. Marinova, *Surf. Coat. Technol*. **2004**, *446*, 180.
[9] Y. Zhou, J. A. Switzer, *J. Alloys Compd*. **1996**, *237*, 1.
[10] I. Zhitomirsky, A. Petric, *Ceram. Int*. **2001**, *27*, 149.
[11] I. Zhitomirsky, A. Petric, *Mater. Lett*. **1999**, *40*, 263.
[12] M. Balasubramaniam, C. A. Melendres, A. N. Mansour, *Thin Solid Films* **1999**, *347*, 178.
[13] L. Martínez, E. Román, J. L. de Segovia, S. Poupard, J. Creus, F. Pedraza, *Appl. Surf. Sci*. **2011**, *257*, 6202–6207.
[14] C. S. Linz, S. K. Fang, *J. Electrochem. Soc*. **2005**, *152*, B54.
[15] M. Hosseini, H. Ashassi-Sorkhabi, H. A. Yaghobkhani Ghiasvand, *J. Rare. Earth* **2007**, *25*, 537.
[16] S. Poupard, F. Pedraza, J. Creus, *Defect Diffusion Forum* **2009**, *289–292*, 235.
[17] Y. Hamlaoui, F. Pedraza, C. Rémazeilles, L. Tifouti, *Mater. Chem. Phys*. **2010**, *120*, 172.
[18] Y. Hamlaoui, F. Pedraza, L. Tifouti, *Corros. Sci*. **2008**, *50*, 2182.
[19] Y. MA, Y. Li, F. Wang, *Corros. Sci*. **2009**, *51*, 997.
[20] D. Guergova, E. Stoyanova, D. Stoychev, I. Avramova, P. Stefanov, *J. Rare. Earth*. **2015**, *33*, 1212.
[21] E. Michailova, M. Peykova, D. Stoychev, A. Milchev, *J. Electroanal. Chem*. **1994**, *366*, 195.
[22] D. J. Mac Kinnon, J. M. Brannen, *J. Appl. Electrochem*. **1982**, *12*, 21.
[23] L. K. Wu, L. Liu, J. Li, J. M. Hu, J. Zhang, C. Cao, *Surf. Coat. Technol*. **2010**, *204*, 3920.
[24] V. Moutarlier, B. Neveu, M. P. Gigandet, *Surf. Coat. Technol*. **2008**, *202*, 2052.
[25] L. M. Palomino, P. H. Suegama, I. V. Aoki, M. F. Montemor, H. G. De Melo, *Corros. Sci*. **2009**, *51*, 1238.
[26] X. Li, S. Deng, H. Fu, G. Mu, *Corros. Sci*. **2009**, *51*, 2639.
[27] X. Li, S. Deng, H. Fu, G. Mu, *Corros. Sci*. **2008**, *50*, 3599.
[28] B. Bouchaud, J. Balmain, G. Bonnet, F. Pedraza, *J. Rare Earth*. **2012**, *30*, 559.
[29] Y. Hamlaoui, F. Pedraza, C. Remazeilles, S. Cohendoz, C. Rébéré, L. Tifouti, J. Creus, *Mater. Chem. Phys*. **2009**, *113*, 650.
[30] Y. Hamlaoui, H. Boudellioua, L. Tifouti, F. Pedraza, *J. Mater. Eng. Perform*. **2015**, *24*, 4626.

[31] H. Boudellioua, Y. Hamlaoui, L. Tifouti, F. Pedraza, *J. Mater. Eng. Perform*. **2017**, *26*, 4402.
[32] M. Ferreira, Jr., K. P. Souza, F. M. Queiroz, I. Costa, C. R. Tomachuk, *Surf. Coat. Technol*. **2016**, *294*, 36.
[33] T. D. Golden, A. Q. Wang, *J. Electrochem. Soc*. **2003**, *15*, C621.
[34] O. Yu. Zelenin, *Russ. J. Coord. Chem*. **2007**, *33*, 346.
[35] M. K. Marchewka, A. Pietraszko, *J. Phys. Chem. Solids* **2005**, *66*, 1039.
[36] G. H. Annal Therese, P. Vishnu Kamath, *J. Appl. Electrochem*. **1998**, *28*, 539.
[37] Y. Matsumoto, J. Hombo, *J. Electroanal. Chem*. **1990**, *279*, 331.
[38] L. Arurault, P. Monsang, J. Salley, R. S. Bes, *Thin Solid Films* **2004**, *446*, 75.
[39] L. Aries, *J. Appl. Electrochem*. **1994**, *24*, 554.
[40] Ph. Refait, C. Bon, L. Simon, G. Bourrié, F. Trolard, J. Bessière, J. M. R. Génin, *Clay. Miner*. **1999**, *34*, 499.
[41] J. Creus, F. Brezault, C. Rébéré, M. Gadouleau, *Surf. Coat. Technol*. **2006**, *200*, 4636.
[42] J-P. Viricelle, *PhD. Thesis*, Ecole Nationale Supérieure des Mines de Saint-Etienne, (French) **1994**.
[43] P. Mani, S. Suresh, *Rasayan J. Chem*. **2009**, *2*, 307.
[44] S. Marcelin, N. Pébère, S. Régnier, *Electrochimica Acta*. **2013**, *87*, 32.
[45] E. A. El-hafian, E. S. Elgannoudi, A. Mainal, A. H. Yahaya, *Turk. J. Chem*. **2010**, *34*, 47.
[46] Y. Hamlaoui, F. Pedraza, L. Tifouti, *Corros. Sci*. **2008**, *50*, 2182.
[47] D. Guergova, E. Stoyanova, D. Stoychev, I. Avramova, P. Stefanov, *J. Rare Earth*. **2015**, *33*, 1212.
[48] J. M. Ferreira, J. L. Rossi, M. A. Baker, S. J. Hinder, I. Costa, *Int. J. Electrochem. Sci*. **2014**, *9*, 1827.
[49] Y. Ma, Y. Li, F. Wang, *Corros. Sci*. **2009**, *51*, 997.

How to cite this article: Bourenane N, Hamlaoui Y, Remazeilles C, Pedraza F. Effect of the pH of the electrolyte on the formation and on the corrosion properties of ceria based coating on carbon steel. *Materials and Corrosion*. 2018;1–10. https://doi.org/10.1002/maco.201810302